Astron. Astrophys. 349, 573–587 (1999)

ASTRONOMY AND ASTROPHYSICS

On the nature of the H I infrared emission lines of τ Scorpii⋆

P.A. Zaal[1], A. de Koter[1], L.B.F.M. Waters[1,2], J.M. Marlborough[3], T.R. Geballe[4], J.M. Oliveira[5,6], and B.H. Foing[5]

[1] Astronomical Institute Anton Pannekoek, University of Amsterdam, Kruislaan 403, 1098 SJ Amsterdam, The Netherlands
[2] SRON Laboratory for Space Research Groningen, P.O. Box 800, 9700 AV Groningen, The Netherlands
[3] Department of Physics and Astronomy, University of Western Ontario, London, Ontario, N6A 3K7, Canada
[4] Joint Astronomy Center, 660 N A'ohoku Place, Hilo, Hawaii 96720, USA
[5] ESA Space Science Department, SCI-SO/ESTEC, PB 299, 2200 AG Noordwijk, The Netherlands
[6] Centro de Astrofísica da Universidade do Porto, Rua das Estrelas s/n, P-4150 Porto, Portugal

Received 17 December 1998 / Accepted 13 July 1999

Abstract. We present Hα, He I λ 2.058 μm and 6 hydrogen Brackett and Pfund lines of τ Sco (B0.2V) obtained using the ground-based INT and UKIRT instruments as well as satellite data from ISO. The infrared lines all show core emission. We have investigated the formation of these lines using sophisticated non-LTE models.

The observed emission in the most pronounced hydrogen lines, such as Brα and Pfα, is stronger than predicted by our models. The velocities of peak emission are blue-shifted by 5–10 km s^{-1} with respect to the stellar velocity. This together with the surprisingly strong width of Brα and the peculiar profile of He I λ 2.058 suggests that shock-induced turbulent velocity fields may be present in or somewhat above the stellar photosphere, as has already been suggested from analysis of optical and ultraviolet data. We derive $T_{\rm eff}$ = 32$\pm$2 kK from the infrared data alone, a value consistent with previous optical analysis. The good agreement indicates that quantitative analysis of infrared lines alone (e.g. for hot stars in regions of high extinction) can be used to characterize photospheres accurately. We also investigate the mass loss of τ Sco and find an upper-limit of 6 10^{-9} $M_\odot$yr^{-1}.

A parameter study of the infrared hydrogen and helium lines indicates that emission may be expected in Brα and Pfα for stars with $T_{\rm eff} \gtrsim 16$ kK and will dominate the profiles of these lines for $T_{\rm eff} \gtrsim 31$ and 26 kK, respectively. He I λ 2.058 will be in emission for $20 \lesssim T_{\rm eff} \lesssim 33$ kK and He II line profiles will contain emission at $T_{\rm eff} \gtrsim 33$ kK. The effect of surface gravity on these values is small.

Key words: stars: atmospheres – stars: early-type – stars: emission-line, Be – infrared: stars – line: formation – radiative transfer

Send offprint requests to: P.A. Zaal

⋆ based on data obtained with the ESA Infrared Space Observatory (ISO), with the UK infrared telescope (UKIRT, Hawaii) and with the Isaac Newton Telescope (INT, La Palma)

1. Introduction

Quantitative spectroscopy is a powerful method to obtain information on the physical conditions that prevail in stellar atmospheres. Theoretical models for stellar atmospheres and their synthetic spectra are widely used to determine basic stellar parameters such as $T_{\rm eff}$, $\log g$, projected rotational velocity and chemical composition. The technique of quantitative spectroscopy is of particular interest when applied to the infrared (IR) wavelength band. As extinction properties of interstellar and/or circumstellar dust are not nearly as severe in the IR as compared to the visual, the IR allows for the study of hot stars located in regions of high optical extinction. Examples are the star forming sites in the Galactic disk and the hot stars located in the galactic center.

In particular, the IR part of the spectrum of hot stars contains a wide range of strong and weak hydrogen and helium lines that are formed in the outer layers of the static atmosphere, and in the lower parts of the stellar wind. The strength and shape of these lines are very sensitive to the structure of the atmosphere, and hence provide strong constraints on model atmospheres in a region that is difficult to probe with other techniques (Najarro et al. 1998).

In recent years, the IR part of the spectrum has become accessible to quantitative spectroscopy due to the development of large IR arrays, and the launch in 1995 of the Infrared Space Observatory (ISO). We have embarked on an observational study of the IR spectra of hot stars, in order to (i) observationally characterize hot stars in the IR, (ii) derive basic parameters of hot stars, and (iii) derive information about the circumstellar material in hot stars (either in outflows or in disks).

The MK standard star τ Sco (HD149438, Sp. Type: B0.2 V) is one of the best studied hot stars and is very bright, allowing high quality observations. τ Sco shows enhanced stellar wind features for its spectraltype (Walborn et al. 1995). However, its derived mass mass loss rate of 1–3 10^{-8} M$_\odot$ yr^{-1} (Lamers & Rogerson 1978; Kudritzki et al. 1989) is not expected to effect optical and IR lines (see Sect. 4.3). This allows us to investigate the *photospheric* IR spectrum. The effective temperature and $\log g$ for τ Sco are 31.4 kK and 4.24 respectively (Kilian 1992).

Peters & Polidan (1985) and Lamers & Rogerson (1978) derive comparable values. Waters et al. (1993) first reported the presence of strong Brα emission in τ Sco, and attributed this emission to the presence of a low-density disk. However, subsequent studies by Murdoch et al. (1994) showed that the emission in τ Sco and in the O9V star 10 Lac can also be understood in terms of non-LTE (LTE = Local Thermodynamic Equilibrium) line formation in a plane-parallel atmosphere, without the need for circumstellar gas.

In this paper we present new ground-based and space-based optical and IR spectroscopy of τ Sco that confirm the emission character of the cores of many IR hydrogen lines (as well as He I λ 2.058), pointing to significant non-LTE effects in the line-forming regions. In Sect. 3, we present new non-LTE model atmosphere calculations (H&He models) for hot stars. Sect. 4 discusses the physical mechanisms responsible for the formation of emission line cores in the IR lines of plane-parallel hot-star atmospheres. Sect. 5 discusses the mass loss of τ Sco and the extent to which this is expected to affect the IR lines. Here we also address the possibility the observed IR line emission is due to the presence of a (low-density) disc. In Sect. 6 we present convenient diagnostic diagrams to compare the line strengths of the IR lines to observations, and we compare the models on which these diagrams are based to the observed lines of τ Sco Also a comparison is made between fully line blanketed and H&He models. Finally, Sect. 7 summarizes the results of this paper.

2. The observations

Spectra of τ Sco were obtained in both the optical and IR spectral range. They cover mainly hydrogen and helium lines. The description of the observations and the data reduction is divided into three parts: the optical INT Hα spectrum; the ground-based UKIRT spectra; and the ISO spectra. All spectra discussed below are corrected for the motion of the earth, the Sun and a stellar radial velocity of $+2$ km s^{-1} (Hoffleit & Jaschek 1982).

2.1. The INT data

An Hα spectrum was obtained in 1996 May 2nd with the Isaac Newton 2.5m Telescope (INT) on La Palma during the commissioning run of the MUSICOS spectrograph. In total the spectrograph has 50 orders covering the spectral range 4718–8139 Å. To obtain the Hα spectrum we extracted the order which covered the wavelength interval 6527–6626 Å. The spectral resolving power, $R = \lambda/\delta\lambda$, for this spectral range is 3.0 10^4. The data were reduced with the MIDAS echelle reduction package, using standard reduction steps for echelle spectra: order definition, order extraction and wavelength calibration (Th-Ar spectrum). The Hα line is normalized using a 2nd order polynomial fit through the continuum.

The normalized Hα spectrum is shown in Fig. 1 and derived spectral parameters are given in Table 1. The wings of the line show blends of He II 6−4 at -132 km s^{-1} (relative to Hα) and C II at $+695$ and $+917$ km s^{-1}. Comparing the absorption profiles of the blue and red wing suggests that the He II line is dominated by emission.

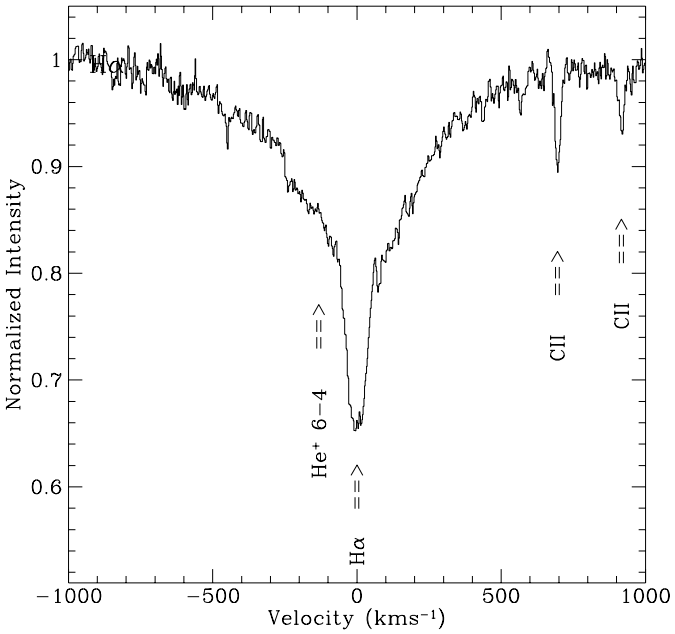

Fig. 1. Hα observed in 1996 May 2nd with INT during commissioning of the MUSICOS instrument.

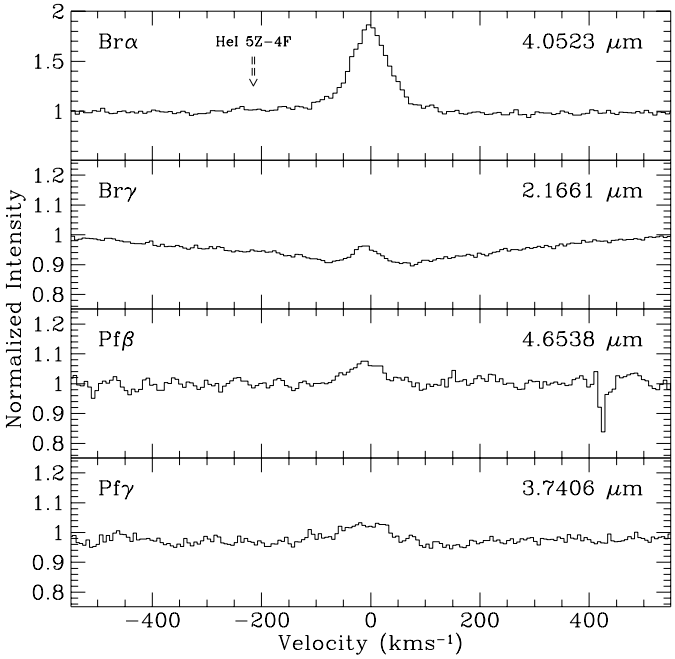

Fig. 2. UKIRT observations of hydrogen emission profiles in τ Sco.

2.2. The UKIRT data

United Kingdom Infrared Telescope (UKIRT) spectra were obtained over two observing runs using the echelle of the facility grating spectrometer, CGS4. The first two spectral ranges shown in Fig. 2, centered on Brα (4.052 μm) and Brγ (2.17 μm), are

Table 1. Basic parameters of the observed line profiles. Given are the spectral resolution, the line over continuum ratio, I_l/I_c, at peak velocity v_{peak}, the equivalent width (EW), the full width at half maximum (FWHM) of the feature, the signal to noise ratio and the telescope used. A negative (positive) EW means net emission (absorption). The error in v_{peak} is $\approx$ 1/10 the velocity characteritic for the spectral resolution.

Line	Resolution	I_l/I_c	E.W. (Å)	Line flux (W/m^2)	v_{peak} (kms^{-1})	FWHM (kms^{-1})	S/N	Telescope/ Instrument
Hα	36000	0.65	3.0	–	0	200	100	INT/MUSICOS
Brα	14000	1.86	−10.3	−1.53e-15	−4	71	75	
Brγ	15000	0.96	5.2	–	−14	–	220	
Pfβ	15000	1.07	−1.0	–	−14	70	80	UKIRT/CGS4
Pfγ	15750	1.04	1.6	–	−11	–	110	
He I λ 2.058	18700	1.12	−0.4	–	21	40	50	
Brα	2017	1.5	−12	1.8e-15	−10	150	100	
Brβ (a)	2070	0.96	4.3	−5.7e-15	10	200	40	ISO/SWS AOT02
Brβ (e)		1.05	−0.7	5.4e-16	20			
Pfα	1457	1.4	−23	3e-16	0	206	20	

observed on July 4th 1994 and are reduced as described by Zaal et al. (1997). The spectral coverage is about 1500 kms^{-1} for each spectrum. The last two spectral ranges, covering Pfγ (3.740 μm) and Pfβ (4.653 μm), were taken on July 26th 1995. With the 256 x 256 InSb array installed previously in that year, the spectral coverage is much larger: about 4000 kms^{-1} for each spectrum. Similar specifications apply for the He I $2p^1S-2s^1P^\circ$ (2.058 μm) line shown in Fig. 3. In order to subtract the telluric lines we used R CrB (HD141527, Spt G0Iep) as ratio star for the Pfγ and Pfβ spectrum. For the He I spectrum we used HR6366 (HD154783, Spt A/Fm). The Pfγ and Pfβ spectra suffer from fringing. These were removed with the defringe tool "FRINGEAAR" as developed for the data reduction of the SWS-ISO data and which is part of the Interactive Analysis package. The derived spectral parameters are given in Table 1.

For all spectra shown in Fig. 2 we find the (local) emission feature to peak at a negative velocity (see Table 1). Moreover, all lines are slightly asymmetric in that they show enhanced emission at the violet side of the profile. As pointed out by Zaal et al. (1997) this indicates that at the depths where the (non-LTE) line centers are formed there is an overall outward (line of sight) velocity. In the case of Brα we add that He I λ 4.049 (at -234 kms^{-1} from Brα) is suspected to be in emission. In the case of Pfβ we note that the absorption at $+420$ kms^{-1} is a residual from a strong telluric line.

The He I λ 2.058 line is situated in a difficult atmospheric window, as a series of strong telluric lines is present. The raw spectra are shown in the lower panel of Fig. 3. A slight shifting of the position of the ratio star in the slit in the dispersion direction has a large impact on the shape of the intrinsic line profile. The equivalent width of the line, however, is conserved. The shape difference is illustrated in the top two tracings shown in Fig. 3. For a 0.2 pixel shift (1.1 kms^{-1}) the overall residuals of the telluric lines are minimal. Independent on the shift of the ratio star we find that line emission is only present at positive velocities. We detected also weak He I emission at $+287$ kms^{-1} relative to He I λ 2.058. Comparison between model calculations and the observed He I spectrum shows that the red-shifted emission in He I is real, i.e. the weaker He I line velocity is zero relative to the local standard of rest velocity of τ Sco (see Fig. 13). In this paper we will only use the He I spectrum as derived *with* shifting the ratio star.

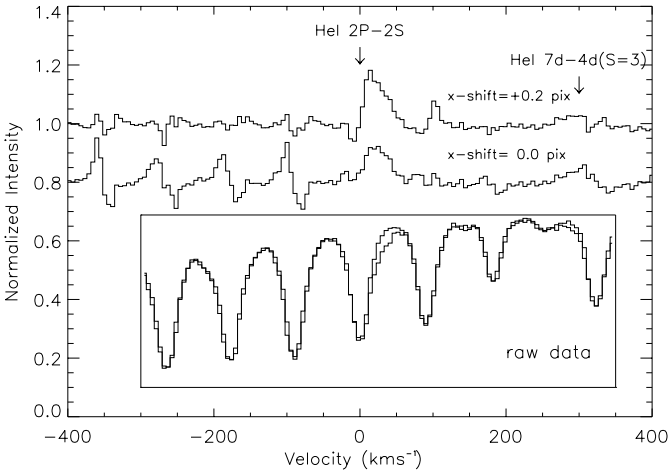

Fig. 3. The He I 2.058 μm spectrum as observed with UKIRT. The top spectrum as reduced with a slight shift of 0.2 pixel (1.1 kms^{-1}) for the ratio star, HR6366. The bottom spectrum as reduced without shifting the ratio star. Also the"raw" spectra of τ Sco and HR6366 are given to illustrate the strong telluric lines present.

2.3. The ISO data

We observed τ Sco with the Short Wavelength Spectrograph (SWS) on board of the Infrared Space Observatory (de Graauw et al. 1996; Kessler et al. 1996). The SWS was used in the SWS02 mode. The aperture size is $14''$ x $20''$ for the spectral range covered by our observations. The spectral resolution, which is wavelength dependent and ranges from $\lambda/\delta\lambda \approx 1400$ to 2100, is given in Table 1. The spectra as shown in Fig. 4 were reduced using the SWS Interactive Analysis (IA) programs within Interactive Data Language (IDL).

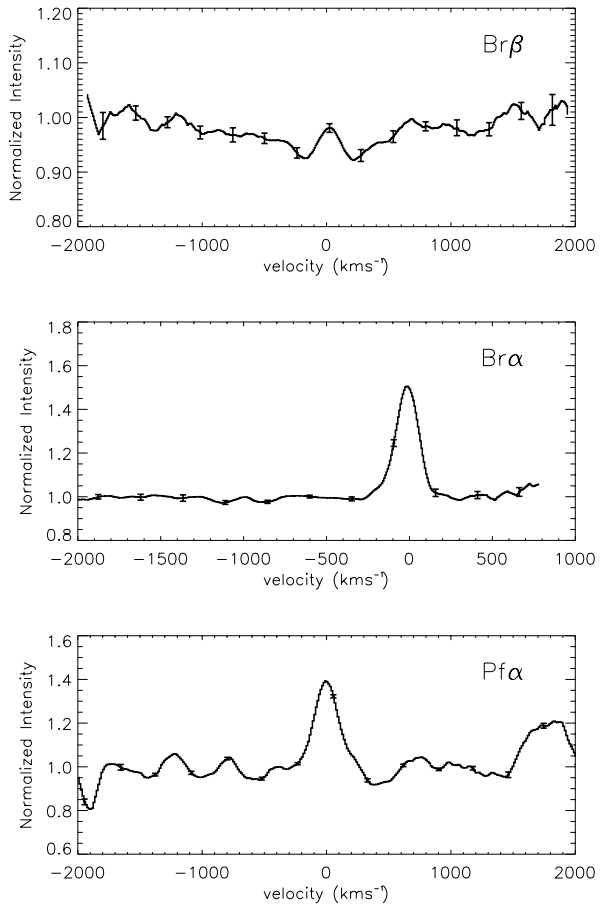

Fig. 4. ISO observations of IR hydrogen profiles in τ Sco.

The applied data reduction is quite different from the standard pipeline in that we make use of the algorithms developed by Valentijn & Thi (1999). These algorithms are specifically developed in order to detect weak lines. The algorithms address the problem that the dark current often shows drifts on various time scales as well as sudden jumps in the mean level. Due to cosmic ray hits both the dark current and the science data show glitches. Such glitches can be detected as sudden jumps in a series of ramp slopes (the so called "maxi-glitches") or as a small jump within a particular ramp ("mini-glitches"). These can be identified using the standard deviation of ramp fits. The data processing of Valentijn & Thi (1999) also makes use of self-calibration, i.e. to define the pulse shape from the science data, which results in a better linearization of the ramp. Globally the algorithm first filters out the glitches and uses the darks which are not affected by glitches to do the dark current subtraction employing a polynomial fit.

We observed τ Sco three times for optimizing the signal to noise ratio (S/N) of various lines. From this data set the spectra with the best S/N were selected. Brα was taken on February 17th 1996, Brβ on September 17th 1996 and Pfα on March 8th 1998. Due to the poor signal to noise of the Pfβ line spectrum we will not include this line in our analysis. Instead we use the Pfβ spectrum obtained with UKIRT. The reduced ISO spectra are shown in Fig. 4. The spectral parameters are given in Table 1. The Brβ profile shows a weak emission feature on top of broad absorption wings. The Brα emission, which is just resolved, looks similar to the Brα spectrum as observed with UKIRT. It shows an asymmetric emission peaking at $\sim -10 \pm 10$ kms^{-1} and the blue emission wing is stronger and extends up to larger velocities than that of the red wing. The measured equivalent width of Brα differs significantly ($\sim$ 14%) from that of the UKIRT data (see Table 1). We cannot conclusively say that this variability is due to calibration problems; it is likely intrinsic. For Pfα, the spectral resolution is much lower than at Brα (see Table 1) and no asymmetry can be detected. As the Pfα spectrum suffers from fringes the actual S/N is lower than the error in Fig. 4 (i.e. noise per bin) indicates. The fringes, clearly visible at ~ -1000 kms^{-1}relative to Pfα, could not be devided out as the S/N in the fourier domain was too low to detect the fringe period. The H I 8$-$6 line at $+1715$ kms^{-1} relative to Pfα is in emission. We did, however, not use this H I 8$-$6 in our analysis as the edges of the observed ISO spectra are poorly covered and thus have too low S/N. Furthermore many He I lines are situated around Pfα. The strongest are at -1115, -895 and -168 kms^{-1} relative to Pfα. Also He II 12$-$10 is seen at -135 kms^{-1}. None of these helium lines are detected, implying they are at least weaker than 15 percent of the continuum although the latter two lines might be stronger as they blend with Pfα.

3. The model calculations

To model the IR lines of τ Sco, we use the non-LTE atmosphere code TLUSTY (Hubeny 1988; Hubeny & Lanz 1995) version 195. The statistical equilibrium equations for hydrogen and helium are solved subject to the constraints of radiative and hydrostatic equilibrium. The atmosphere is assumed to be plane-parallel. We first constructed a grid of H&He model atmospheres covering a broad range in $T_{\rm eff}$ and $\log g$. In order to account for all relevant recombination and cascading channels, we made use of quite extended atomic models. Details of the levels included and the treatment of the transitions between them are given below. In the calculated grid of models the effect of line blanketing, i.e. the consistent treatment of thousands of spectral lines of ions of species other than H&He is neglected. Blanketing effects, however, may be of importance (Lanz et al. 1997) and we will return to this point in Sect. 4 and 5. Line profiles were calculated using the spectral synthesis code SYNSPEC. The H I and He II line profiles are computed as described by Hubeny et al. (1994). For the He I line profiles we use a "classical" profile implying the Stark broadening is approximated by a Voigt profile, with $\Gamma = 10^8\ n_{\rm e}\ n_{\rm eff}^5$, where $n_{\rm e}$ is the electron density and $n_{\rm eff}$ is the effective quantum number defined in the usual way.

To get an overview of how IR H I and He I lines depend on effective temperature and $\log g$, and to see in which way non-LTE effects influence the line shapes, we have first set up a grid of models ranging from 16 to 40 kK in $T_{\rm eff}$ with a stepsize of 2 kK and in $\log g$ using values from 3.7 to 4.3 with a stepsize of 0.15. All other parameters are kept fixed. The results of this

first step will be discussed in Sect. 5. Here, we will summarize model ingredients especially important for IR lines.

3.1. Atomic physics

The hydrogen model atom consists of 15 explicit levels, while higher levels, up to $n = 80$, are merged into an averaged non-LTE level accounting for level dissolution as described by Hubeny et al. (1994). The highest members ($n > 15$) of the Lyman and Balmer line series are then represented by their respective transitions to this merged level and are represented by means of opacity distribution functions.

The He II model atom treats the first 14 levels explicitly. He I is represented by a 69 level atom, which treats all levels up to quantum level $n = 7$ and angular momentum $L \leq 3$ separately. The levels with $L > 3$ are grouped into a superlevel for each main quantum number up to $n = 7$. From levels $n \geq 8$ and $n \leq 20$ the singlet and triplet levels for a given quantum level are grouped into single superlevels. Allowed bound-bound transitions of He I (having an Einstein A_{ul} coefficient $> 10^4$) are treated in full non-LTE while forbidden transitions are assumed to be in radiative balance. In this way the most important line transitions of He I are treated consistently and cover all transitions of concern for the analysis presented in this paper. Atomic transition probabilities for the bound-free and bound-bound transitions of He I are from the Opacity Project TOPBASE database (Cunto & Mendoza 1992) for all levels up to quantum level $n = 4$. For levels $n > 4$ we use a hydrogenic approach for the bound-free transitions and the atomic data of Martin (1987) for the bound-bound transitions, kindly supplied by Paco Najarro (private communication).

To check the sensitivity of the He I lines to the used atomic data, we performed a test using different sources of atomic data used for transitions between lower levels, $n_l \leq 3$ and upper levels, $n_u \geq 4$. In this test, we created a new He I atomic model using the Opacity Project data up to $n = 3$ and Martin's data (1987) for $n \geq 4$ and compared this with a run using our standard He I atomic data as described above. A model atmosphere with $T_{\rm eff}$ = 32 kK and $\log g$ = 4.0 was used. No significant change was found in relatively strong H I and He I profiles including He I λ 2.058. Only for the weak He I λ 4.049 μm line emission at -230 km s^{-1} from the center of Brα (see Fig. 2) a decrease of about 30 percent in line strength was predicted in case Martin's data was used. One should beware of this problem as it may affect the overall synthetic line profile of Brα (4.052 μm) when convolved to the resolution of the ISO observations.

3.2. The influence of turbulent velocity

In the presented grid of H&He models, effects of small-scale motion fields – generally referred to as "micro-turbulent velocities" have not been taken into account. To investigate the effect of micro-turbulence we performed test calculations treating it in a consistent manner. This implies that turbulence was allowed to *(a)* modify the hydrostatic structure of the model – through an induced turbulent pressure gradient – (e.g. de Jager et al. 1991); *(b)* affect the transfer of radiation – by desaturating the lines. This allows photons to escape from deeper layers, enhancing the non-LTE character (e.g. Sigut & Lester 1996); and *(c)* influence the profile function in the formal solution to recover the line profile.

The test calculations covered the effective temperature range from 28 to 34 kK and $\log g$ from 3.7 to 4.3. We assumed $v_{\rm turb}$ = 10 km s^{-1}. For H I IR lines we found an overall enhancement of the line emission. Besides the increase of the line width due to mechanism *(a)*, also the line over continuum ratio increases due to mechanism *(b)*. As a result the equivalent width of these lines decreased (i.e. more line emission) by some 20 percent for all models. The $v_{\rm turb}$ effect on He I λ 2.058 and Hα is more complex. We will return to this in Sect. 5.1. The neglect of turbulence may lead to an overestimate of the effective temperature by approximately 400 K (assuming 10 km s^{-1} is realistic). The effect on $\log g$ is not significant.

4. The formation of emission lines due to non-LTE effects

In this section we will discuss the formation of IR emission lines in terms of simple physics.

4.1. The principle of non-LTE line emission

In a plane-parallel atmosphere line emission may occur either through a temperature inversion or through a non-LTE effect in which the upper level of the transition gets overpopulated relative to the lower level. We will briefly discuss the principle of both effects. The important point we want to show is that it requires only a small deviation of the ratio between the non-LTE departure coefficient of the upper and lower level from unity (i.e. LTE) to cause a spectral line to go into emission. Anticipating the results of the model calculations, we note that in τ Sco the population inversion is the more important of the two effects.

The line source function between upper level u and lower level l is given by:

$$S_{l,\nu_o} = \frac{2h\nu_o^3}{c^2}\left[\frac{b_l}{b_u}\exp\left(\frac{h\nu_o}{kT_e}\right) - 1\right]^{-1} \quad (1)$$

where ν_o is the line frequency; $b_n = n/n^*$ denotes the departure of the level population n from the LTE value n^*, and T_e is the electron temperature. The constants have their usual meaning. We assume the continuum to originate from a layer with characteristic temperature T_e^* and to emit a radiation field given by the Planck function. Normalizing the line source function to this continuum background yields:

$$\frac{S_{l,\nu_o}}{B_{\nu_o}} = \frac{\exp(h\nu_o/kT_e^*) - 1}{\frac{b_l}{b_u}\exp(h\nu_o/kT_e) - 1} \quad (2)$$

To first order Eq. (2) gives the peak strength of the emission line if the temperature T_e is characteristic for the layer in which the line becomes optically thick at its central wavelength.

Let us first discuss the temperature inversion effect. To do so, we assume b_u/b_l=1. For a spectral line located in the IR we

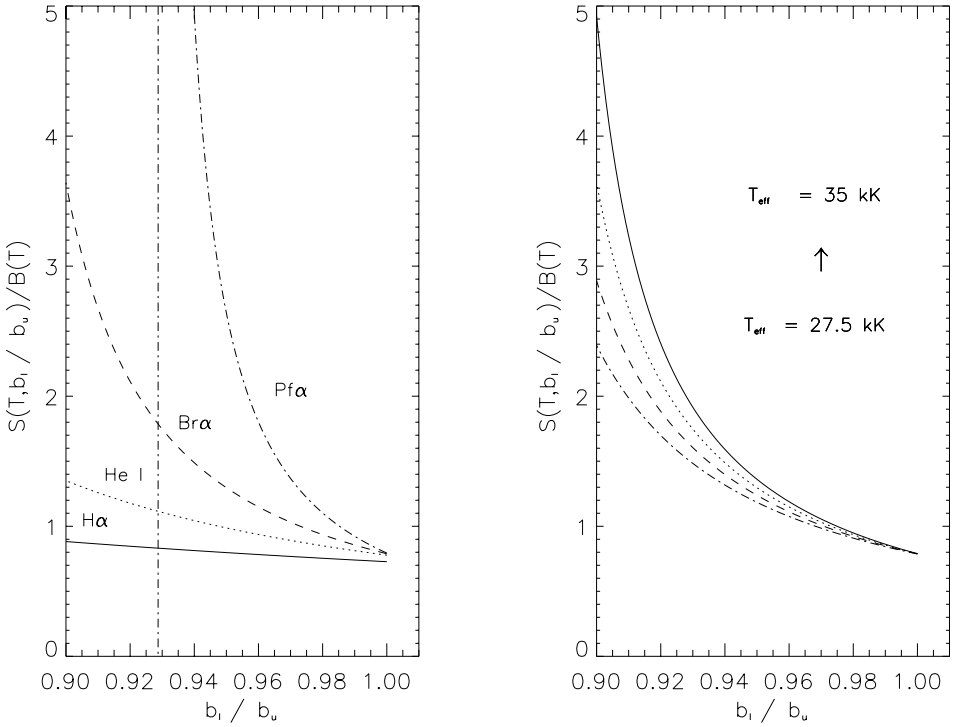

Fig. 5. The left panel shows the dependence of the line over continuum source function ratio, $S_{l,\nu}/B_\nu$, as a function of b_l/b_u for Hα, He I λ 2.058, Brα, and Pfα. Characteristic temperatures are T_e^* = 32.5 kK and T_e = 0.8 T_e^*. The right panel shows the dependence as a function of stellar effective temperature for Brα. Four values are indicated, $T_{\rm eff}$ = 27.5, 30, 32.5 and 35 kK.

may apply the Rayleigh-Jeans approximation. This reduces the expression for the continuum normalized line source function to $S/B = T_e/T_e^*$, i.e. the peak strength scales linearly with the ratio of the temperatures. This implies that in case $T_e > T_e^*$ in the line forming region one may expect an emission profile. Temperature inversion occurs in our H&He model atmospheres.

We now turn to the population inversion effect. In Fig. 5a we present for our simple model the ratio S/B for different ratios b_u/b_l assuming T_e/T_e^* = 0.8. The different lines are for Hα, He I λ 2.058, Brα, and Pfα. Fig. 5a clearly shows that for the IR lines only a few percent difference in b_u and b_l yields significant peak emission. Line amplification is small for the optical Hα line, essentially because the exponential temperature behaviour dominates the line source function at short wavelengths. The photospheric temperature dependence is illustrated in Fig. 5b. The strong dependency of emission strength on b_u/b_l in the IR can be simply understood by introducing the following approximation:

$$\frac{S_{l,\nu_o}}{B_{\nu_o}} = \frac{1}{\frac{b_l}{b_u}\frac{T_e^*}{T_e} + \frac{1}{\delta}\epsilon} \qquad (3)$$

where $\delta = h\nu_{lu}/kT_e^*$ and $\epsilon = b_l/b_u - 1$ (see also Sigut & Lester, 1996). Depending on the sign of ϵ, non-LTE effects can either result in enhanced absorption ($\epsilon > 0$) or in enhanced emission ($\epsilon < 0$). The amplification factor of emission is determined by $1/\delta$. In Sect. 4.2 we will demonstrate that for (several) H I and He I lines of early B-type stars, the value of b_l/b_u can become smaller than unity, i.e. $\epsilon < 0$, in the region of line formation.

One may expect significant emission when $\epsilon < 0$ and $|\epsilon|/\delta \rightarrow b_l/b_u * T_e^*/T_e$ at the depth where the line is formed. We will refer to this effects as "b-amplification". The singularity visible in Fig. 5a in case of Pfα exists because of stimulated emission. Note that in a real stellar atmosphere the emission will be "tempered" by continuum opacity contributions.

The b_u/b_l sensitive population inversion effect is the dominant cause of IR line emission in τ Sco. Other effects that may produce line emission will be discussed in Sect. 5.

4.2. The $T(r)$ and $b_n(r)$ effect within TLUSTY

Details about the formation of Hα, Pfα and He I λ 2.058 in a TLUSTY model are given in Fig. 6. The model parameters are $T_{\rm eff}$ = 31.4 kK and $\log g$ = 4.24 and are characteristic for τ Sco (Kilian 1992). The top three panels give the dependence of temperature, density and the ratio b_l/b_u of the three investigated lines on Rosseland optical depth. The middle set of panels give the continuum (dashed line) and line (solid line) source function. The symbols in the source function plot give the position at which the continuum and line reach monochromatic optical depth 2/3. The bottom row of panels show the emerging line profiles.

Our grid of H&He models exhibits a temperature rise at the surface. This temperature rise is a classical non-LTE effect first described by Auer & Mihalas (1969; see also Mihalas 1978) and is the result of an indirect effect of Balmer lines on the heating in the Balmer continuum. Line blanketed models have the tendency not to show this behaviour because of more efficient cooling through spectral lines in the outer layers. The H&He temperature inversion is of minor importance for weak lines, such as He I λ 2.058, as for weak lines the forming region is typically situated *inside* of the layer where the temperature is $\sim$ 10% above the minimum. For the stronger line transitions, such as Hα, Brα and Pfα, which have a line forming region

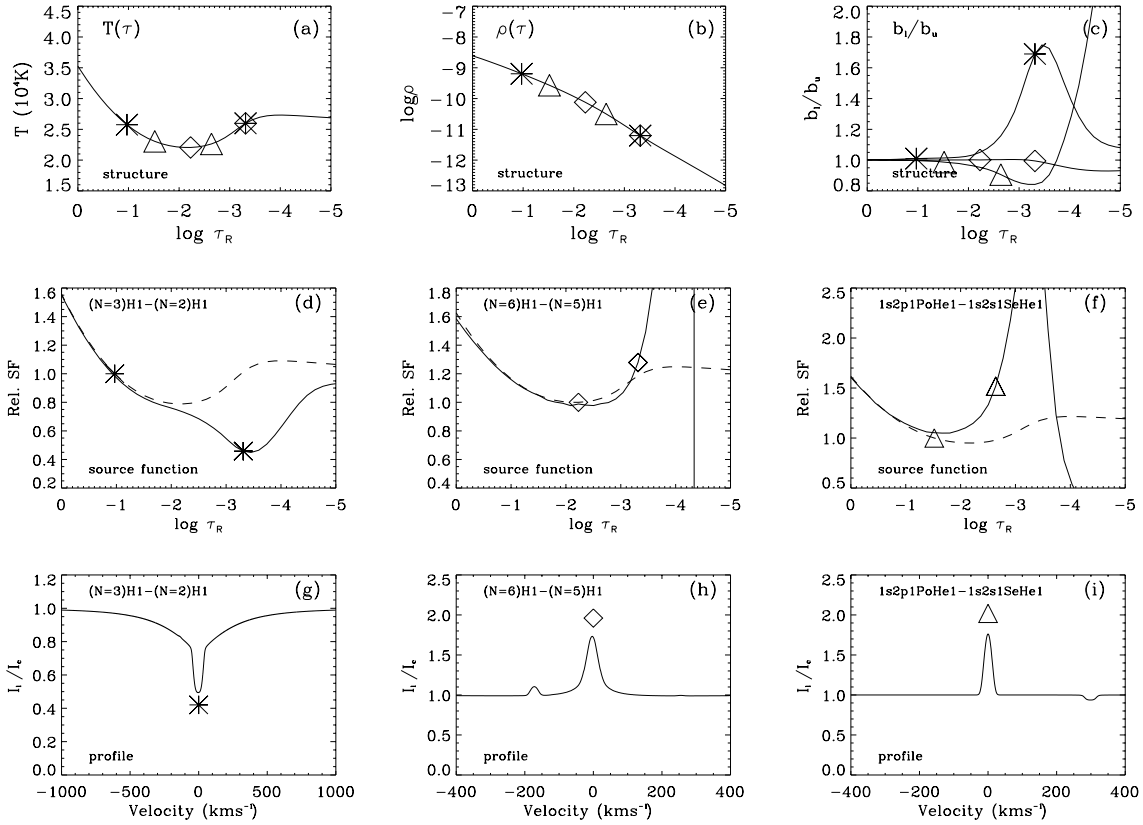

Fig. 6a–i. An overview of the atmospheric structure and of the line and continuum source functions for three lines: Hα, Pfα and He I λ 2.058. The bottom three panels show respective predicted line profiles. Information about different lines is indicated with different symbols. Data are for a TLUSTY model atmosphere with $T_{\rm eff}$ = 31.4 kK and $\log g$ = 4.24. The top panels show the run of temperature, density and b_l/b_u with depth. Marked are the positions where line core and continuum reach optical depth τ = 2/3. The non-LTE line (solid line) and continuum (dashed line) source functions given in the middle three panels are normalized to the continuum source function value at continuum τ = 2/3.

extending *beyond* the temperature inversion, the rise in temperature is expected to be of importance. For these strong lines the temperature in the line forming region is typically more than 10% above the minimum. We will return to this in Sect. 5.

In the case of Hα, clearly the line to continuum source function ratio (at τ = 2/3 in line and continuum respectively) is less than unity and absorption line is the result (see Fig. 6d). Interestingly, Fig. 6a shows that the temperature in the continuum and line forming layer is about equal. This implies that it must hold that in the line forming layer $b_2/b_3 > 1$, which is confirmed in Fig. 6c. The main part of the central line depression can be explained by the model ratio $b_2/b_3 \simeq 1.5$. The continuum at Pfα is formed farthest out of the three lines shown in Fig. 6. Actually, it originates at about the temperature minimum at $\log \tau_{\rm Ross} \sim -2$ (Fig. 6a). The core of the line is formed around the temperature maximum. We find $T_e/T_e^* \sim 1.22$. This explains part of the predicted line emission in Pfα, reaching a peak strength of $\sim$ 1.7 (Fig. 6h). The second effect of importance is the amplification of the line over continuum source function ratio. This is nicely illustrated in Fig. 6e. At around the line core formation region one sees a steep increase in this ratio, while Fig. 6c shows that the ratio b_5/b_6 deviates only slightly from unity. Also for He I λ 2.058 the "*b*-amplification" effect is the dominant reason why the line is in emission. Unlike Pfα the temperature inversion effect does not help to boost the line (Fig. 6a). Both continuum and line core are formed in the regime of the temperature minimum. Note that the amplification effect is again nicely demonstrated by the behaviour of the line source function plotted in Fig. 6f. This function reaches a sharp maximum at $\log \tau_{\rm Ross} \sim -3$. The line core is formed on the slope of this maximum.

5. Alternative effects that may produce IR emission lines

In principle, IR emission lines may also be produced by material in a circumstellar disc or in a stellar wind. In this section, we will discuss the validity of these scenarios.

5.1. Emission from a circumstellar disc around τ Sco

For rapidly rotating B-type stars with $v\sin i > 230\,{\rm km\,s^{-1}}$ Bjorkman & Cassinelli (1993) expect disc formation. For such a disc stellar UV photons may ionize the gas and depending on the local temperature and density recombination may give rise to line emission in the optical and IR. Indeed, about 10% of the O9/B2 stars are known to have Hα emission (Jaschek & Jaschek 1983). If the viewing angle of the disc is close to edge-on, this gives

rise to double-peaked line emission; if seen pole-on, a relatively sharp emission lines are expected such as seen in τ Sco. Zaal et al. (1995) pointed out that low-density discs can give rise to H I IR emission without having significant emission in Hα. The density and temperature in these low-density discs are comparable to the temperature and density in the formation region of the IR lines in our H&He models. This suggests that line formation in a low-density disc may also be affected by non-LTE effects. However, we do not expect the IR line-emission in τ Sco to be the result of a disc. Zaal et al. (1997) showed that 7 out of 8 slowly rotating stars in their sample ($v\sin i < 50$ km s^{-1}), including τ Sco, show single peaked emission in Brα. Since it is not likely all these stars have a pole-on low-density disc, the most likely (and simple) interpretation for the IR line emission of H and He is photospheric.

5.2. The stellar wind of τ Sco

The mass loss rate of τ Sco has been derived by Lamers & Rogerson (1978) assuming the rapid acceleration of the gas is due to radiation pressure in UV-resonance lines. They derive a mass loss rate of 7 10^{-9} M$_\odot$ yr^{-1} using ultraviolet lines such as C III, C IV, N III, N V, Si IV and O VI. We re-investigated the mass loss of τ Sco three different ways: *(i)* by modelling the $\dot{M}$-sensitive Si IV resonance line using non-LTE unified model atmospheres; and *(ii)* by applying the analytical solutions of radiation driven wind theory.

5.2.1. $\dot{M}$ using unified model analysis

The presented models are calculated using the most recent version of the non-LTE unified Improved Sobolev Approximation code ISA-WIND for stars with stellar winds (de Koter et al. 1993; de Koter et al. 1997, 1998). Here, we will not discuss model assumptions, input atomic physics nor numerical methods, which are treated in detail in the above mentioned references. We suffice to say that detailed atomic models are included for H, He, C, N, O, Si and S and that line blending by iron-group elements is included in the formal solution yielding the synthetic spectrum. The adopted effective temperature and $\log g$ values are from Kilian (1992). The stellar radius is derived using the Hipparcos distance (ESA 1997). Adopting a bolometric correction BC= -3.06 (Kurucz 1991), the derived bolometric luminosity implies a radius R_* = 4.7 $R_\odot$. The applied stellar parameters are as given by Kilian (1992); the terminal flow velocity v_∞ = 2000 km s^{-1} is adopted from Lamers & Rogerson (1978) and corresponds to the maximum blueshift in the C IV resonance doublet. We assumed a β-type velocity law with β=0.5. This value implies a steeper velocity law than that typical for OB-type stars where $\beta \sim 0.8$. However, this value reproduced the absorption part of the Si IV $\lambda\lambda 1393, 1403$ best.

Note that we did not attempt to do a complete non-LTE wind analysis. In contrast, we concentrated solely on fitting the Si IV profile using an IUE spectrum as supplied by the INES server of the IUE archive in Vilspa (Barylak & Ponz 1998). Si IV is a sensitive mass loss diagnostic and has the advantage over, e.g. the N V and C IV resonance lines, that its ionization is not expected to be influenced by shock induced soft X-ray emission (e.g. Lucy & White 1980). Fig. 7 compares the observed Si IV profile (thick line) of τ Sco with predicted line profiles (thin lines) assuming five different mass loss rates, $\dot{M}$ = 4, 6, 8, 10 and 15 10^{-9} $M_\odot$yr^{-1}, respectively. The lines may be distinguished easily as an increasing $\dot{M}$ yields progressively more absorption at large blueshifts. Interestingly, wind absorption sets in first at the terminal velocity. One may easily understand this applying Sobolev theory: the radial line optical depth at given wavelength in the observers frame is proportional to $n_i(dv/dr)^{-1}$. In the case of τ Sco the small velocity gradient close to where the terminal speed is reached – compared to, say, the lower regions of the wind – dominates over the decrease of the Si IV population. Consequently, one first reaches $\tau \sim 1$ at large velocity. In this way we derive an upper limit to the mass loss of $\sim$ 6 10^{-9} $M_\odot$yr^{-1}. This number is very similar to the mass loss rate derived by Lamers & Rogerson (1978). We note that the derived upper limit is a very sensitive function of effective temperature. Test calculations show that if T$_{\rm eff}$ = 33 kK, then the ionisation of Si will have changed so dramatically that $\dot{M}$ can only be constrained to be less than 10 10^{-9} $M_\odot$yr^{-1}. Similarly, if T$_{\rm eff}$ = 30 kK, the mass loss should be less than 4 10^{-9} $M_\odot$yr^{-1}.

5.2.2. $\dot{M}$ using radiation driven wind theory

We used the analytical solution for radiation-driven winds of Kudritzki et al. (1989) to predict the mass-loss rate of τ Sco. In this formulation, the line force is expressed in terms of three distance-independent force multiplier parameters, k, α and δ. Ideally, the values of the force multipliers should be obtained from detailed full multi-level non-LTE calculations. Pauldrach et al. (1990) were the first to perform such calculations for a grid of models representative for early-type stars. From their grid, we adopt $k = 0.024$, $\alpha = 0.737$ and a typical value $\delta = 0.1$ for force multiplier representing the ionization balance throughout the wind. The predicted mass loss is 5.3 10^{-9} $M_\odot$yr^{-1} for an adopted mass of 12 M$_\odot$. This result is close to the upper limit derived from the Si IV profile. Cohen et al. (1997) use line-force parameters calculated by Abbott (1982) and derive $\dot{M}$ = 3.1 10^{-8} $M_\odot$yr^{-1} for the mass loss of τ Sco. The large discrepancy is mainly due to the significantly different luminosity adopted by these authors.

6. Results

The outcome of the TLUSTY model calculations over a wide range in T$_{\rm eff}$ and $\log g$ give a good indication of the regime in which to expect IR line emission in hot stars. To facilitate this overview we first present T$_{\rm eff}$ – $\log g$ contour plots of the equivalent width (EW) of selected synthetic line profiles. These EW's are compared with those observed in τ Sco. The fundamental question we want to address is whether one may determine basic stellar parameters using IR lines only. In a second step we take a closer look at the corresponding line profiles over this range in T$_{\rm eff}$ and $\log g$. Finally a comparison between the outcome of

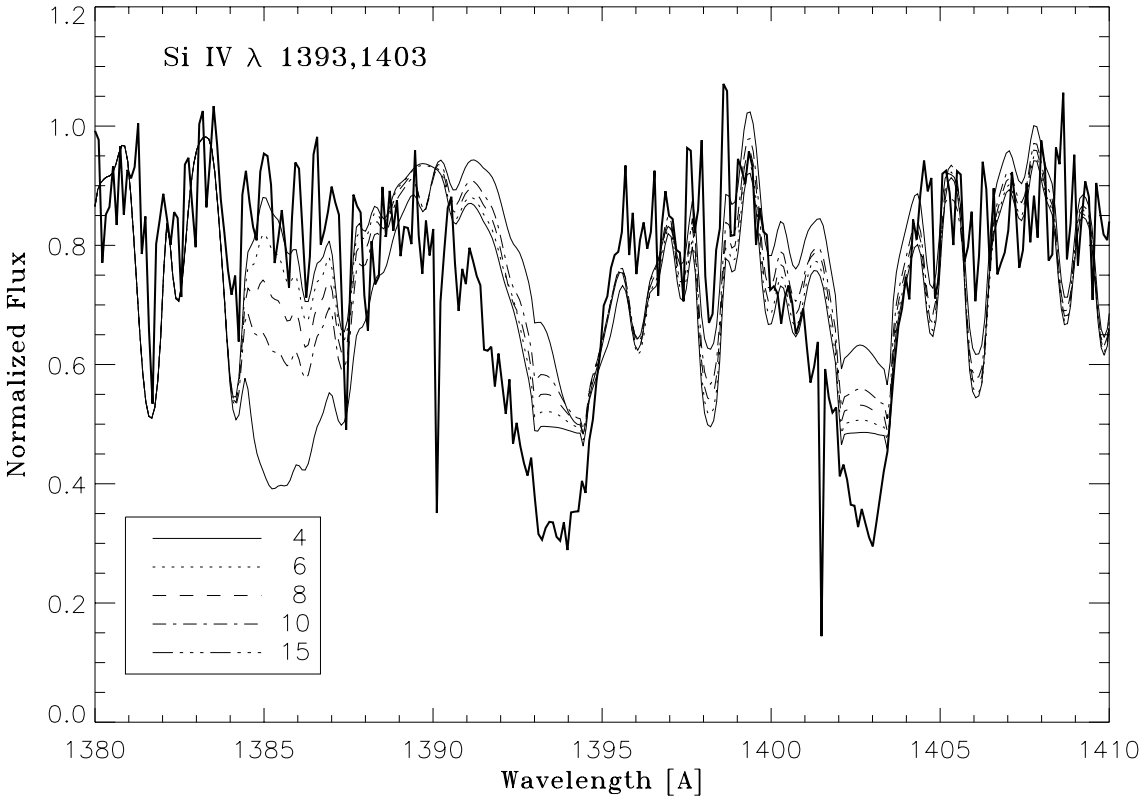

Fig. 7. The observed Si IV line profile of τ Sco and the synthetic spectra as derived with the ISA-WIND code for five different mass-loss rates, given in the legend in units of 10^{-9} $M_{\odot}\mathrm{yr}^{-1}$. Increasing $\dot{M}$ yields progressively more absorption at large blueshifts, which can be used to derive an upper limit of the mass-loss rate of $\sim 6\ 10^{-9}$ $M_{\odot}\mathrm{yr}^{-1}$.

our H&He model and a fully line blanketed model for τ Sco is made.

6.1. The equivalent width dependence on $T_{\rm eff}$ and $\log g$

The H&He models span the range $T_{\rm eff} \in$ [16,40] kK and $\log g \in$ [3.7,4.3]. τ Sco, for which we adopt $T_{\rm eff}$ =31.4 $\pm$ 0.3 kK and $\log g$ = 4.24 $\pm$ 0.03 (Kilian 1992), is situated well within this range. We will use the model grid to address two questions. First, in which part of parameter space may one expect IR emission lines? Second, can these lines be used to derive basic stellar parameters? The latter question is of particular interest for the study of hot stars located in regions of high extinction, such as e.g. OB-stars embedded in their natal clouds or located in the galactic center.

In Fig. 8 we show the synthetic equivalent width contours of the eight lines observed for τ Sco. The EW's are measured between $-/+$ 300 $\mathrm{km\,s^{-1}}$ from line center, except for the broad Hα profile for which we used an interval between $-/+$ 1000 $\mathrm{km\,s^{-1}}$. To facilitate the comparison between observed and predicted EW's, we re-measured the observed values using the same wavelength intervals. In principle, these re-measured EW's may differ from those given in Table 1 if absorption is present beyond $-/+$ 300 $\mathrm{km\,s^{-1}}$. The adopted bounds guarantee that for all IR lines the central emission is included. This does not holds for the wings of the lines. However, we did not want to extend the bounds further as a larger bound would lead to larger errors in the EW as a result of the uncertainty in the continuum level. The hydrogen lines Pfα, Pfβ and Brα show net emission, starting at about 26, 30.5 and 30.8 kK respectively. At lower $T_{\rm eff}$ the lines show net absorption, but core emission is present. This is also the case for the weaker hydrogen lines like, Brβ, Brγ and Pfγ. The EW of Hα, dominated by the absorption wings, gradually decreases (i.e. less absorption) with increasing ionization, i.e. increasing effecive temperature. For $T_{\rm eff} \gtrsim 34$ kK non-LTE effects starts to become important at large depths leading to an increase of the width of the central absorption. This again results in an increase of the equivalent width (i.e. more absorption). He I λ 2.058 shows line emission from a $T_{\rm eff}$ of 16 to 33 kK due to the "b-amplification" effect. At $T_{\rm eff} \lesssim 16$ kK LTE prevails and the line is in absorption. At $T_{\rm eff} \simeq 33$ kK, where helium starts to be double ionized, the line again turns into absorption. For this last regime we find that $b_l/b_u > 1$, i.e. non-LTE enhances the absorption.

From Fig. 8 we may conclude that *emission profiles of photospheric origin* for Pfα, Pfβ and Brα may be observed from spectral type B2–3 extending to earlier types assuming these lines are fully resolved (say $\lambda/\delta\lambda \gtrsim 5000$). In all the lines the gravity dependence is very weak, except for Hα. This implies that the EW of the IR emission lines can be used *only* as a sensitive $T_{\rm eff}$ diagnostic. For determining $\log g$ they lack this predictive power. In Sect. 6.2 we will show that the $\log g$ sen-

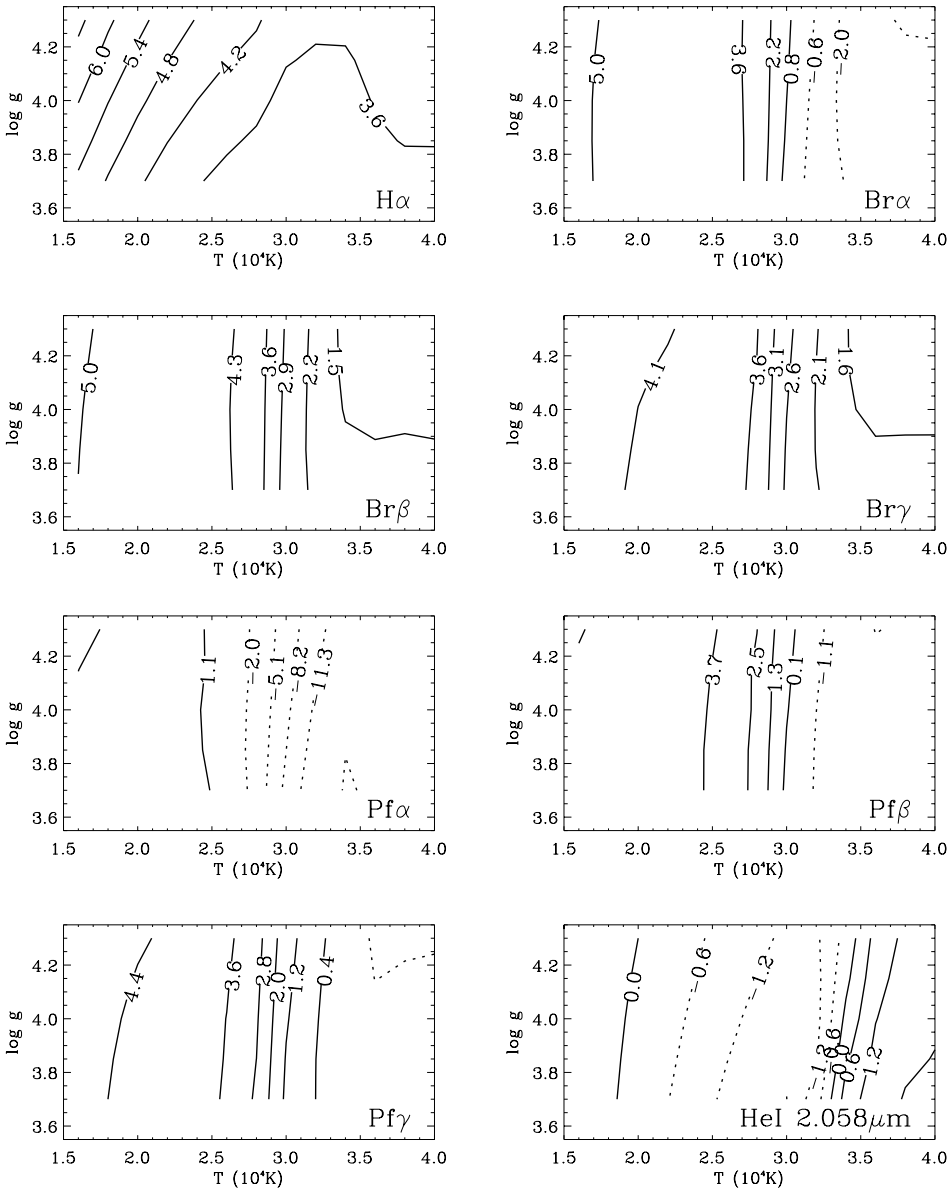

Fig. 8. Predicted $T_{\rm eff}--\log g$ contour plots for eight line profiles. The contours represent the equivalent width (in Å) of the line profiles between $-/+$ 300 $\mathrm{km\,s^{-1}}$, except for Hα where we used an interval between $-/+$ 1000 $\mathrm{km\,s^{-1}}$. Solid (dashed) lines indicate net absorption (emission).

sitivity can be improved by selecting a different bound for the EW measurement. For stars with spectral type earlier than O9 ($T_{\rm eff} \gtrsim 34$ kK) the investigated IR spectral lines will start to be affected by stellar winds. This also holds for the late O- and early B-type giants and supergiants (Najarro et al. 1998). In these cases one needs to include the stellar wind in the model calculations to predict realistic line strengths.

The contours in the $T_{\rm eff}$–$\log g$ diagram as given in Fig. 9 represent the photospheric parameters as derived from H&He model calculations using the observed (re-measured) EW's. By combining all the different contours we try to derive a $T_{\rm eff}$ for τ Sco. The EW's of Pfβ, Pfγ, Brβ and He I λ 2.058 are all consistent with a temperature $T_{\rm eff} = 32 \pm 2$ kK. This is in agreement with the 31.4 ± 0.3 kK as derived by Kilian (1992). The observed EW of Brγ, which is dominated by relatively strong Stark broadened wings matches a lower $T_{\rm eff}$ of about 28 kK. Interestingly, the observed EW values of Hα, Brα and Pfα are considerably off compared to those derived with the H&He models. The mismatch in Hα may mainly be ascribed to the central absorption, which is not as strong as predicted by the non-LTE calculations. Also the observed EW's of Brα and Pfα (see Table 1) are considerably smaller (i.e. stronger in emission) and are not within the plot range of Fig. 9. We investigate two possible causes for this discrepancy. First, we study the effects of small scale turbulent velocities. Second, we explore the differences between H&He and more sophisticated line-blanketed model atmospheres.

As shown in Sect. 3.2 a higher $v_{\rm turb}$ enhances the strength of the line. An increase in $v_{\rm turb}$ from $0 \rightarrow 10$ $\mathrm{km\,s^{-1}}$ results in an overall shift of -400 K in $T_{\rm eff}$ and $+0.04$ in $\log g$ in Fig. 9. Although such a $v_{\rm turb}$ shifts the EW of the synthetic spectra slightly closer to observed values, it is not enough to explain the apparent discrepancy between the two.

A second possible explanation for the discrepancy may be the neglect of effects of line blanketing. The effect of including

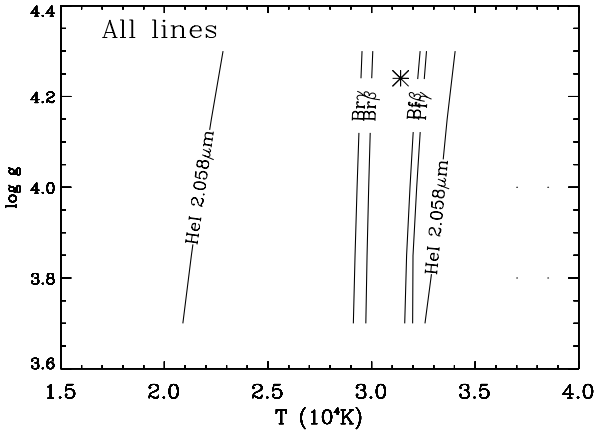

Fig. 9. $T_{\rm eff} - \log g$ diagram in which for each line are plotted the contours where the predicted equivalent width matches the observed one. Predictions are based on H&He models. The $*$-symbol indicates the basic parameters of τ Sco as determined by Kilian (1992), i.e.$T_{\rm eff}$ = 31.4 $\pm$ 0.3 kK and $\log g$ = 4.24 $\pm$ 0.03. For He I λ 2.058 the EW matches two contours as the predicted EW shows a maximum at $\sim$ 25–30 kK (see Fig. 8). The observed EW of Hα, Brα, and Pfα fall outside the range of this plot (see text).

line blanketing on the photospheric structure is complex as it may change the temperature structure as well as the excitation and ionization structure, sometimes through subtle mechanisms (e.g. Schmutz 1997). Studying the difference in temperature structure between H&He and line blanketed models may already give insight in the effect of blanketing on line profiles.

In general, line blanketing heats the inner photosphere and cools the outer layers, removing the temperature inversion present in H&He models. Line blanketed models show a higher temperature at the point of formation of the local continuum and a steeper temperature gradient over the line forming region compared to the structure in a H&He model. Consequently, line profiles show an enhanced absorption in case LTE applies as is often the case for the line wings. For instance, in the case of Brγ, which shows strong absorption wings, blanketing strongly affects the derived EW. An overall comparison between the non-blanketed and blanketed models (see Sect. 6.3) shows that line blanketing enhances "*b*-amplification".

6.2. The dependence of the line profile on $T_{\rm eff}$ and $\log g$

In this section we will discuss line shapes. Unfortunately, a parameter study using blanketed models only is – in view of computational costs – not yet feasible. We therefore show trends of the profiles in $T_{\rm eff}$ and $\log g$ using H&He models. In Figs. 10 and 11 we show the temperature behaviour for eight different line profiles. For each spectrum four different temperatures have been plotted, i.e. $T_{\rm eff}$ = 28, 30, 32 and 34 kK respectively. The value for the gravity was kept fixed at $\log g$ = 4.3.

Fig. 10 shows the relatively weak Brβ, Brγ, Pfβ and Pfγ profiles. With increasing effective temperature the central line emission increases as non-LTE effects become more enhanced. For the same reason the line wings decrease in (absorption) strength. Brα and Pfα, presented in Fig. 11, are dominated by a central emission. Here also, the emission increases with increasing $T_{\rm eff}$. Over the whole range in $T_{\rm eff}$ the line center of Hα is strongly affected by non-LTE, resulting in an enhancement of the central absorption. At $T_{\rm eff}$ = 34 kK a slight inversion in the line core is visible. The absorption strength at line center decreases for increasing $T_{\rm eff}$, contributing to a decrease in EW. At $T_{\rm eff} > 34$ the EW of Hα starts to increase as non-LTE effects become more import at larger depths, increasing the width of the central absorption. He I λ 2.058 shows a maximum strength at $T_{\rm eff}$ = 30 kK. The line profile for $T_{\rm eff}$ = 34 kK demonstrates the depth dependence of b_l/b_u, i.e. this ratio shows a minimum in the line forming region.

Fig. 8 shows that the dependence on $\log g$ for the EW of H I IR lines is weak compared to the dependence on $T_{\rm eff}$. For an effective temperature, $T_{\rm eff}$ = 30 kK Fig. 12 shows the $\log g$ dependence for four line profiles: Brα, He I λ 2.058, Pfβ and Pfγ. Different than Fig. 8 suggests, the H I IR line profiles do show a significant gravity dependence: both the core emission and the wing absorption increase with decreasing $\log g$. The He I λ 2.058 dependence on $\log g$ is weak compared to the H I lines.

Because we have chosen the velocity range over which to calculate the equivalent width rather broad ($-/+$ 300 km s^{-1}), the line core and line wing effect tend to cancel out the $\log g$ sensitivity in the EW determination. For decreasing $\log g$ the contribution of the extra core emission is canceled by the slightly stronger absorption in the line wings. Although the EW sensitivity of the H I lines is dominanted by temperature, the $\log g$ sensitivity can slightly be improved by decreasing the bounds to about $-/+$ 60 km s^{-1}(assuming the central emission to be resolved). Furthermore, if one decrease the effective temperature, $T_{\rm eff} \lesssim 30$ kK, the $\log g$ dependence for the H I IR lines tends to become weaker. For $T_{\rm eff} \gtrsim 30$ kK the $\log g$ dependence slightly increases, most notably for Pfβ and Pfγ.

6.3. Comparison of observed and predicted profiles

In order to assess the importance of line blanketing, we compared a H&He model and a line blanketed model using the literature values of Kilian (1992) for $T_{\rm eff}$ and $\log g$ (resp. 31.4 kK and 4.24). The latter calculations include a consistent non-LTE treatment for the elements H, He, C, N, O, Si, S, Fe and Ni. For consistency with the relatively simple H&He models, identical hydrogen and helium atomic data was used. Figs. 13 and 14 show a comparion of the synthetic and observed spectrum. The first are convolved to the spectral resolution given in Table 1. The line blanketed spectra show an overal better fit for the wings of Brβ, Pfγ and Brγ. The predicted absorption strength for these lines are much stronger compared to H&He models due to a steeper temperature gradient and because the temperature inversion is removed. This has direct implications for Fig. 9, where we compared the derived EW from the H&He model with observed values. In case line blanketing would have been considered, the derived $T_{\rm eff}$ following from the Brβ, Pfγ and Brγ lines would agree even better with the literature value of

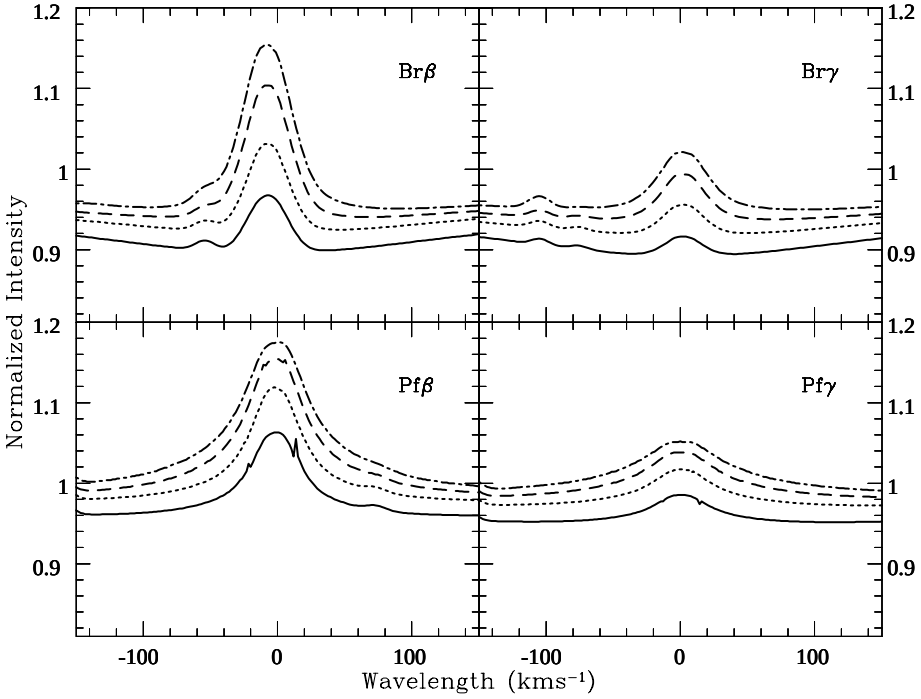

Fig. 10. Profiles of four IR lines (Brβ, Brγ, Pfβ, Pfγ) as predicted using H&He models for four values for $T_{\rm eff}$: 28 kK (solid), 30 kK (dotted), 32 kK (short dashed) and 34 kK (long dashed). Gravity is kept fixed at log g = 4.3.

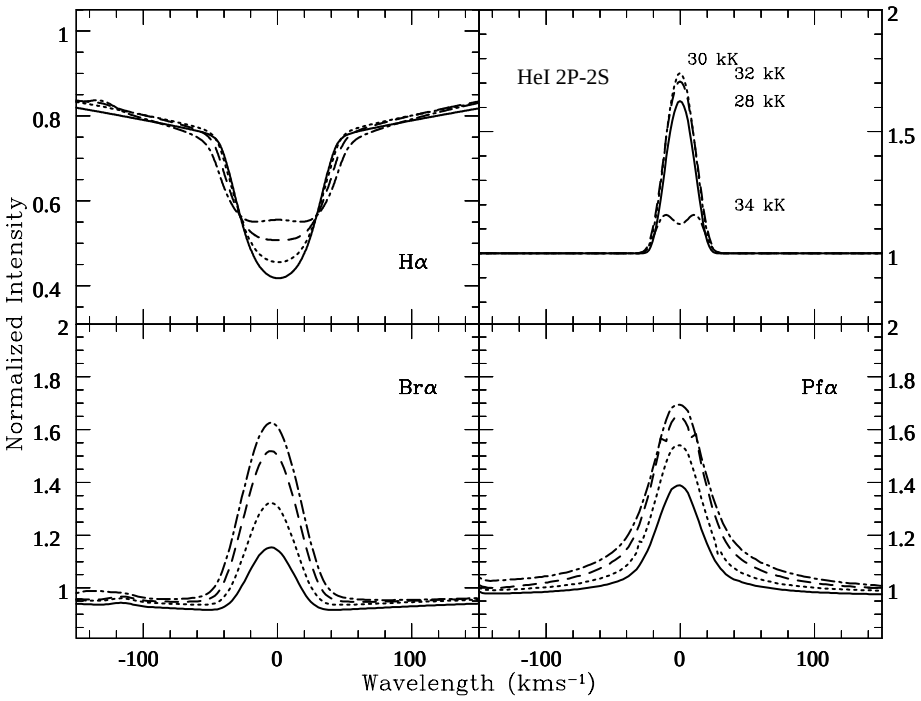

Fig. 11. Effective temperature dependence of Hα, He I λ 2.058, Brα, and Pfα, predicted using H&He models (as in Fig. 10). For He I λ 2.058 the corresponding $T_{\rm eff}$ is given at the level of maximum line flux.

31.4 kK. In case of Hα the core is somewhat better represented when accounting for line blanketing. However, including line blanketing does not improve the fit for the Hα line wings.

The predicted line strength of Brα and Pfα are more similar to that observed, but remain significantly weaker. Fig. 13 shows that Brα is not fully resolved with SWS as the grating resolution is much lower. Although it is clear that the observed line width is broader than predicted by both models. The Brα UKIRT observation – which fully resolves the line – shows the discrepancy in line width much clearer. It shows a half line width of about 200 $\rm km s^{-1}$, whereas the predicted spectra show $\approx$ 50 $\rm km s^{-1}$. The observed line-core over continuum ratio agrees with the value from the line blanketed model and the mismatch in EW for Brα is obviously due to the extra line flux at larger velocities (up to 200 $\rm km s^{-1}$). The discrepancy suggests that high turbulent velocities may be present in the photosphere of τ Sco. Since the Pfα spectrum is also observed with SWS – with a relatively low resolution – we expect that the mismatch in this profile is also intrinsic, i.e. more emission at high velocities should have been predicted. The fit to He I λ 2.058 improves when line blanket-

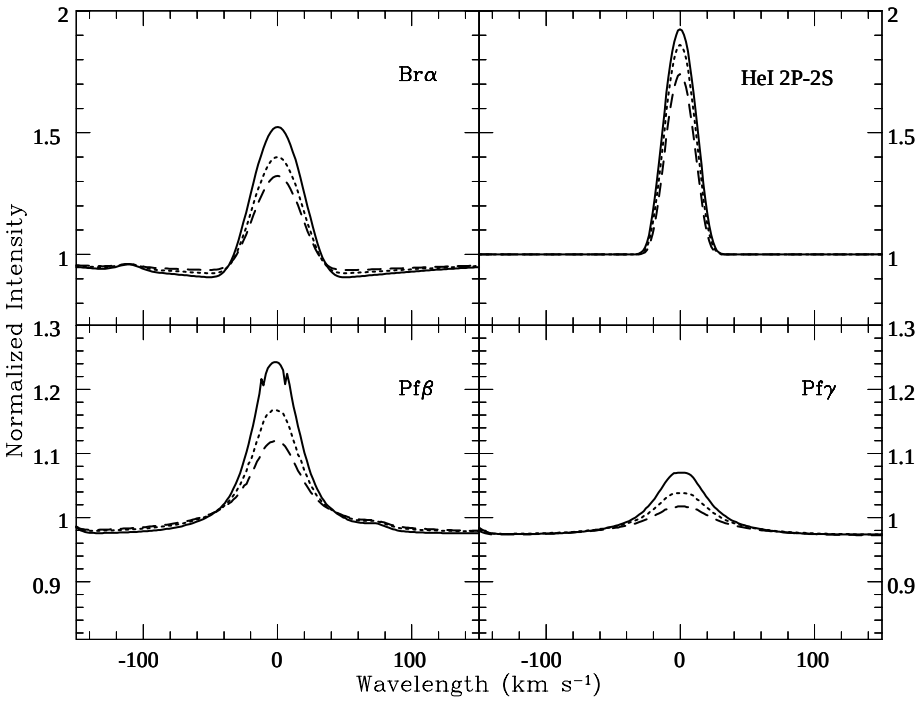

Fig. 12. Gravity dependence of Brα, He I λ 2.058, Pfβ and Pfγ using H&He models. Three values for $\log g$ are used: 3.7 (solid), 4.0 (dotted) and 4.3 (dashed). The effective temperature is kept fixed at 30 kK.

ing is included, although the derived line profile is still far off in shape and line strength. The observed He I λ 2.058 line profile has a peculiar shape. It has an emission profile red-shifted by $\pm$ 20 km s^{-1}. This observed asymmetry can not be a result of an error in the wavelength calibration, as the He I 7d-4d(S=3) line at about +300 km s^{-1} from He I λ 2.058 is at zero velocity. The red-shift suggests that also this line is subject to turbulent and/or large-scale stochastic motions. We note that the H&He and line blanketed models predict the He I 7d-4d(S=3) line – formed relatively deep in the photosphere – to be in absorption. The observed spectrum shows that this line has weak emission.

We conclude that the incorporation of line-blanketing in our non-LTE models gives an overal improvement to the spectral fits. However, the fits of our final blanketed model are not optimal and the peculiar behaviour of some of the IR lines in τ Sco strongly point to the presence of turbulent and/or stochastic velocity fields. An increasing micro turbulent velocity, which is not included in our model calculations, has the effect of enhancing the core emission and increasing the full width half maximum of the line emission (see Sect. 3.2). This is exactly what we need to overcome the mismatch between observations and model spectra of our H I IR lines.

7. Discussion and conclusions

We have investigated the formation of IR emission lines in hot stars using plane-parallel hydrostatic model atmospheres. Such models are expected to be appropriate for early-type stars not showing significant stellar winds, e.g. B-type main sequence stars. We have taken two approaches. First, we have performed a parameter study using non-LTE models consisting of H&He only. Such models may be viewed as present-day "standard" non-LTE models. Second, we have modeled the B0.2V star τ Sco using state-of-the-art line blanketed models.

The grid of H&He models shows that IR emission lines are expected to be most pronounced for Brα and Pfα, which show net emission at $T_{\rm eff} \gtrsim 30.8$ and 26 kK respectively, independent of $\log g$ (see Fig. 8). Core emission in these lines is already present at much lower temperatures ($\pm$ 16 kK). Also He I λ 2.058 and Pfβ show significant central emission in this $T_{\rm eff}$ regime. The models show that two effects may cause this emission. First, it may be due to the presence of a temperature inversion in the outer layers of the atmosphere. Emission due to this effect is more prominent in strong lines such as Brα and Pfα. These lines are of sufficient strength to have their cores formed in the region of increasing temperature. Second, it may be the result of a non-LTE effect referred to as "*b*-amplification". The main constraint for this mechanism is that the line is formed in the Rayleigh-Jeans part of the spectrum. For hydrogen this results in IR core emission for $T_{\rm eff} \gtrsim 16$ kK. For He I it occurs for $20 \lesssim T_{\rm eff} \lesssim 33$ kK and for He II at $T_{\rm eff} \gtrsim 33$ kK.

An important goal of this paper has been to investigate to what extent basic stellar parameters may be derived from IR diagnostics only. Using equivalent widths of several IR lines, we derive an effective temperature for τ Sco of $T_{\rm eff} = 32 \pm 2$ kK, which is consistent with the value of 31.4 ± 0.3 kK derived from a detailed analysis by Kilian (1992) using optical lines. This is an important result in view of the study of hot stars in regions of high extinction. We intent to investigate the robustness of the method applied in this paper to a larger sample of stars. The temperature sensitivity of the IR lines dominates over a modest gravity dependence. A simultaneous determination of both $T_{\rm eff}$ and $\log g$ is therefore difficult. Only if one *adopts* an effective temperature, the cores of the H I lines show a reasonable gravity

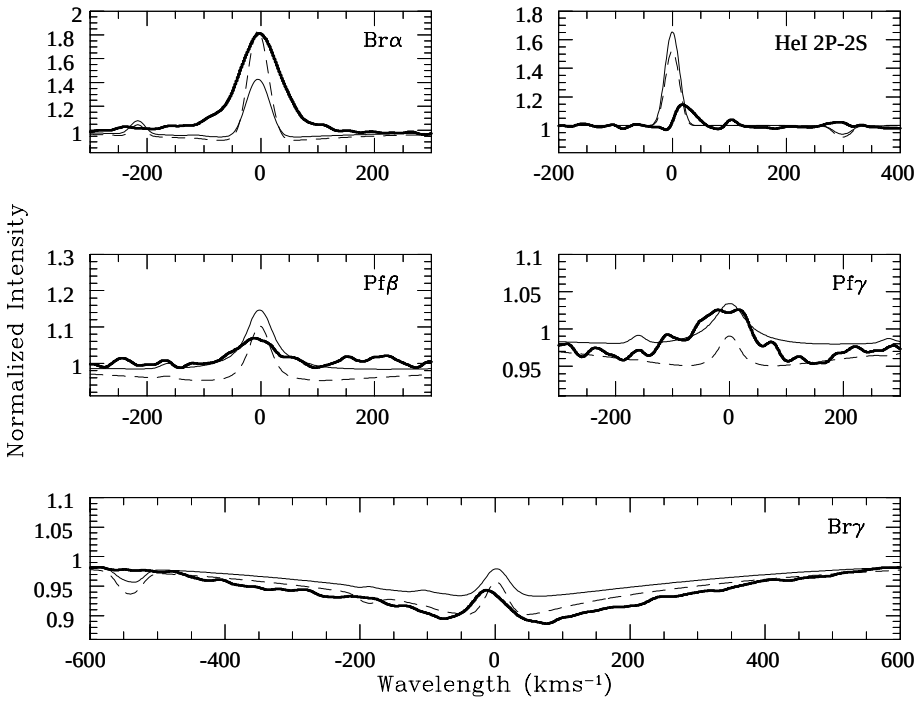

Fig. 13. Comparison between observed INT and ISO spectra and predictions based on a fully line blanketed model (dashed line) and a H&He model (solid line), using $T_{\rm eff}$ = 31.4 kK and log g =4.24. The line blanketed model yields an improved fit to the Brβ profile and helps decrease the discrepancy in Brα.

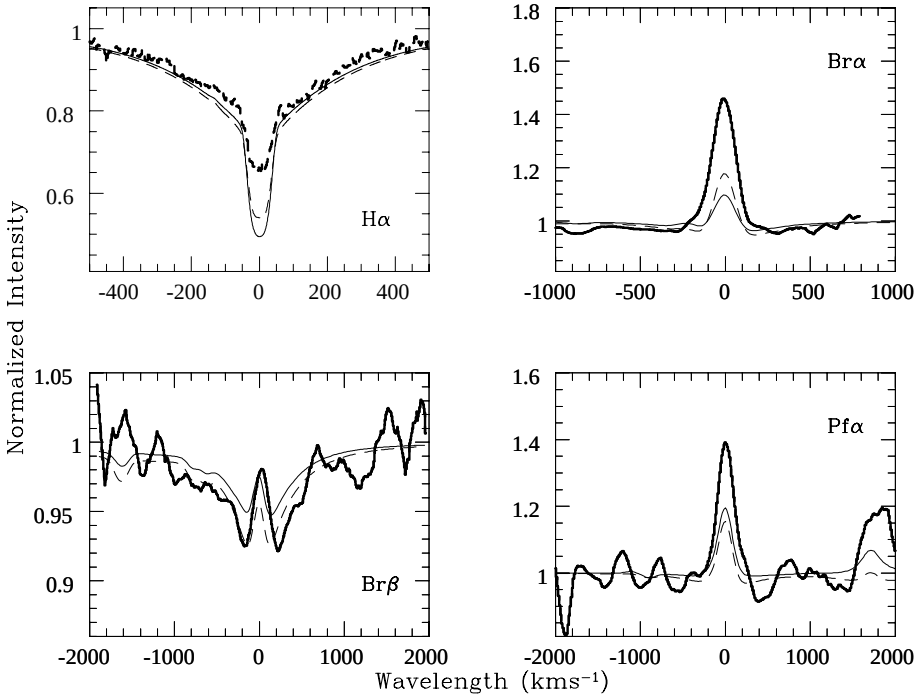

Fig. 14. Comparison of fully line blanketed (dashed line) and H&He model (solid line) with UKIRT observations (as in Fig. 13). The line blanketed model gives an improved fit to Brα and Brγ, but yields a poorer fit to Pfβ.

dependence which (in principle) may allow for a log g estimate. To use the line wings to derive gravity, one requires high S/N observations together with line blanketed models.

Despite its standard star status, τ Sco seems far from normal. High turbulent velocities are found to have effects in the UV (Lamers & Rogerson 1978) and in the optical (Smith & Karp 1978). The star is also a source of X-rays (Swank 1985; Cassinelli et al. 1994) with an unusually hard X-ray spectrum, suggesting the presence of very hot gas ($> 10^7$ K) near the star. These observations imply the atmosphere of τ Sco is complex. The IR spectrum of τ Sco and the O9V star 10 Lac, a star expected to be very similar, have been investigated by Murdoch et al. (1994). They find that 10 Lac gives much better line fits for Brα and Brγ than does τ Sco. This seems to corroborate the complex nature of the atmosphere of τ Sco and warrants further study.

The H&He models with parameters appropriate for τ Sco clearly show emission profiles for those lines observed to be

in emission. This demonstrates that non-LTE effects play an important role in the line formation of IR lines. However, they do not properly reproduce the line strength of the strongest lines (Brα, Pfα), nor do they match the observed widths of these lines.

We investigated to what extent the profile discrepancies might be connected with the neglect of line blanketing or of turbulent velocity fields. Overall the lines fit the line-blanketed model better, but still the model does not properly fit all diagnostic profiles. For instance, the emission in the wings of the resolved Brα line reaches velocities up to $\pm$ 150 km s^{-1}. This is significantly broader than expected and suggests the presence of a strong field of turbulent or stochastic motions, corroborating the results from optical and UV studies. Evidence of bulk motions is also seen. For instance, most H I lines show negative peak velocities of the core emission as well as evidence of enhanced blue-shifted emission. The He I λ 2.058 profile is clearly assymmetric. None of these properties are matched by our models.

Interestingly, the small scale turbulent motions of the order of 100–200 km s^{-1} seen in the line formation regions of Brα and likely Pfα can not be present in the formation region of the UV metal-line spectrum. The photospheric turbulent velocity used in the synthetic spectrum presented in Fig. 7 is 20 km s^{-1}, a value which reproduces the metal-line spectrum around the Si IV resonance line fairly well. A turbulent velocity value of 50 km s^{-1}, however, already it too high producing metal-line widths which are too broad. The unified ISA-WIND model shows that the geometrical difference between the UV and IR formation regimes is about six characteristic density scaleheights of $\sim 4\ 10^{-4}\ R_\star$. The continuum at Brα and Pfα forms just below the sonic point. This implies that the central part of the lines are formed around the sonic point. Apparently, this is where the turbulence first occurs. Such a turbulent velocity profile seems roughly consistent with the shock structure expected from the line-force instability existing in supersonic line-driven outflows (e.g. Owocki 1992, 1994). Detailed numerical simulations of this instability reveal a highly structured wind with many shocks occuring only beyond the sonic point (Feldmeier 1995). This study of τ Sco shows that IR lines may provide important diagnostics for studying these problems.

Acknowledgements. We thank the referee, Paco Najarro, for constructive remarks that have helped improve this paper. We also thank Ivan Hubeny and Thierry Lanz for help setting up the TLUSTY and SYNSPEC code and for computing the line blanketed model. We thank Edwin Valentijn and other members of the ISO team in Vilspa for assistence in reducing the ISO data. We are grateful to the MUSICOS spectrograph group at ESTEC for providing the Hα spectrum. This work was supported by NWO "Pionier" grant 600-78-333 to L.B.F.M. Waters and by Spinoza grant 08-0 to E.P.J. van den Heuvel. JMM and LBFMW acknowledge financial support from a NATO Collaborative Research Grant (CRG.941220).

References

Abbott D.C., 1982, ApJ 259, 282
Auer L.H., Mihalas D., 1969, ApJ 158, 641
Barylak M., Ponz J.D. 1998, in Astronomical Data Analysis Software and Systems VII, ASP Conf. Series, eds. R. Albrecht, R.N. Hook, H.A. Bushouse, Vol. 145, 404
Bjorkman J.E., Cassinelli J.P., 1993, ApJ 409, 429
Cassinelli J.P., Cohen D.H., MacFarlane J.J., Sanders W.T., Welsh B.Y., 1994, ApJ 421, 705
Cohen D.H., Cassinelli J.P., Waldron W.L., 1997, ApJ 488, 397
Cunto W., Mendoza C., 1992, Rev. Mexicana Astron. Af. 23, 107
ESA, 1997, The Hipparcos Catalogue, ESA SP-1200
Feldmeier A., 1995, A&A 299, 523
de Graauw Th., Beintema D.A., Roelfsema P.R., et al., 1996, A&A 315, L49
Hoffleit D., Jaschek C., 1982, Bright Star Catalogue, 4th revised ed., Yale Univ Obs New Haven CT
Hubeny I., 1988, Comp. Phys. Comm., 52, 103
Hubeny I., Lanz T., 1995, ApJ 439, 875
Hubeny I., Hummer D.G., Lanz T., 1994, A&A 282, 151
de Jager C., de Koter A., Carpay J., Nieuwenhuijzen H., 1991, A&A 244, 131
Jaschek C., Jaschek M., 1983, A&A 117, 357
Kessler M.F., Steinz J.A., Anderegg M.E., et al., 1996, A&A 315, L27
Kilian J., 1992, A&A 262, 171
de Koter A., Schmutz W., Lamers H.J.G.L.M., 1993, A&A 277, 561
de Koter A., Heap S.R., Hubeny I., 1997, ApJ 477, 792
de Koter A., Heap S.R., Hubeny I., 1998, ApJ 509, 879
Kudritzki R.-P., Pauldrach A.W.A., Puls J., Abbott D.C., 1989, A&A 219, 205
Kurucz B.L., 1991, in "Precision photometry: astrophysics of the galaxy", October 3–5, 1990, meeting held in Schenectady, New York at Union College, Schenectady, N.Y.: L. Davis Press, p27-44
Lamers H.J.G.L.M., Rogerson J.B., 1978, A&A 66, 417
Lanz T., Hubeny I., Heap S.R., 1997, ApJ 485, 843
Lucy L.B., White R.L., 1980, ApJ, 241, 300
Martin W.C., 1987, Physical Review 36, 3575
Mihalas D., 1978, Stellar Atmospheres (San Francisco: Freeman)
Murdoch K.A., Drew J.E., Anderson L.S., 1994, A&A 284, L27
Najarro F., Kudritzki R.-P., Hillier D.J., et al., 1998, in "ISO's view on stellar evolution", Noordwijkerhout, The Nederlands, 1–4 July 97, Kluwer, eds. Waters L.B.F.M., Waelkens C., van der Hucht K.A., Zaal P.A., p137
Owocki S.P. 1992, in The Atmospheres of Early-Type Stars, eds. U. Heber and S. Jeffery (Heidelberg:Springer), 393
Owocki S.P. 1994, in Instability and Variability of Hot Star Winds, eds. A.F.J. Moffat, A.W. Fullerton, S.P. Owocki, N. St-Louis (Dordrecht:Kluwer),3
Pauldrach A.W.A., Kudritzki R.P., Puls J., Butler K., 1990, A&A, 228, 125
Peters G.J., Polidan R.S., 1985, A&A 152, 182
Schmutz, W., 1997, A&A 321, 268
Sigut T.A.A., Lester J.B., 1996, ApJ 461, 972
Smith M.A., Karp A.H., 1978, ApJ 219, 522
Swank J.H., 1985, in "The Origin of Nonradiative Heating/Momentum in Hot Stars", eds. A.B. Underhill, A.G. Michalitsionos, NASA publ. 2358, 86
Valentijn E.A., Thi W.F., 1999, ISO's Short Wavelength Spectrometer – Ultimate sensitivity, Experimental Astronomy, in press
Walborn N. R., Parker J. W., Nichols J. S., 1995, NASA Ref. Publ. 1363
Waters L.B.F.M., Marlborough J.M., Geballe T.R., Oosterbroek T., Zaal P.A., 1993, A&A 272, L9
Zaal P.A., Waters L.B.F.M., Marlborough J.M., 1995, A&A 299, 574
Zaal P.A., Waters L.B.F.M., Geballe T.R., Marlborough J.M., 1997, A&A 326, 237